Optics and Lasers in Engineering 176 (2024) 108040

Contents lists available at ScienceDirect

Optics and Lasers in Engineering

journal homepage: www.elsevier.com/locate/optlaseng

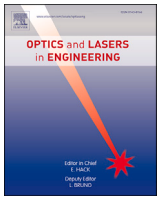

A mode-locked fibre laser temperature independent strain sensor based on intracavity pulse interference

Hani J. Kbashi [a,*], Brian B. Sheil [b], Auro M. Perego [a,*]

[a] Aston Institute of Photonic Technologies, Aston University, Birmingham, B4 7ET, United Kingdom
[b] Laing O'Rourke Centre for Construction Engineering and Technology, Department of Engineering, University of Cambridge, CB3 0FA, United Kingdom

ARTICLE INFO

Keywords:
Laser strain sensor
Mode-locked fibre laser
Mach-Zehnder interferometer

ABSTRACT

High resolution, accurate strain sensors find vital applications in civil, aerospace, and mechanical engineering. Photonic solutions, especially fibre Bragg gratings, despite being promising platforms for strain sensing in harsh environments, and achieving microstrain resolution, suffer from strong sensitivity to temperature fluctuations and require expensive optical detection methods. To tackle these challenges, in this work we present a mode-locked fibre laser strain sensor based on intracavity pulse interference. Our all-fibre sensor, using an intracavity Mach-Zehnder interferometer architecture achieves 20 microstrain resolution with linear response over a 4 millistrain range. Our proposed sensor does not require external locking, and it is environmentally stable, decoupling temperature and strain effects. Furthermore, through a full electronic read-out in radio-frequency domain, our solution can bypass expensive and bulky optical detection. These features pave the way for low-cost and robust photonic strain sensors technology with disruptive real world impact.

1. Introduction

Strain sensing plays a critical role in monitoring the structural health of a wide range of practical applications in aerospace [1], civil [2] and mechanical [3] engineering. A plethora of commercial strain sensing techniques now exist for such applications including foil strain gauges [4], piezoresistive sensors [5], vibrating wire gauges [6], fibre Bragg gratings (FBGs) [7], and distributed optical sensing (e.g. Brillouin time-domain reflectometry [8]). Optical-based strain sensors, in particular, have experienced rapid recent growth for their high sensitivities, invulnerability to electro-magnetic interference and water damage, multiplexing capabilities and long-term stability [9]. However, undesirable thermal sensitivity remains a key challenge and is usually tackled using intricate packaging or cumbersome temperature compensation techniques [10]. This poses a significant barrier to their wider deployment in industry such that there is significant motivation to develop temperature-insensitive optical strain sensors.

Optical frequency combs (OFCs) are emerging in the photonic technology landscape as versatile light sources with prominent applications [11], including greenhouse gas detection [12], distance ranging [13], precision metrology [14], molecular fingerprinting [15], frequency synthesis [16] space exploration and exoplanets search [17,18], optical communications [19], and in advanced phase-sensitive optical time-domain reflectometry techniques for strain and temperature sensing too [20]. OFCs comprise a set of equally spaced coherent frequency laser lines which can be generated in a diverse set of platforms including nonlinear optical resonators [21,22], highly-nonlinear fibres [23], electro-optical modulators [24], optical parametric oscillators [25], hybrid platforms combining active and passive optical cavities [26,27], and mode-locked lasers [28]. In the latter scenario, OFCs are the frequency domain counterpart of ultrashort light pulses circulating inside the optical resonator. A particularly attractive technique is dual-comb spectroscopy [29] which employs two OFCs with slightly different line spacing: one as a probe and the other as a local oscillator. Interference between the OFCs produces a signal in the radio-frequency (RF) domain, thereby circumventing expensive and bulky optical domain detection whilst preserving OFC precision and measurement capability. Despite the vast range of OFC applications, their use for strain sensing has been, so far, limited. Previous research has demonstrated potential for strain sensing using a single OFC. However, such an approach requires an atomic clock for stabilisation, which is also strongly affected by temperature [30], or is based on complicated external synchronisation mechanisms [31]. Various dual-comb mode-locked laser sources have been instead used to interrogate FBGs strain sensors [32–37],

* Corresponding authors.
E-mail addresses: h.kbashi@aston.ac.uk (H.J. Kbashi), a.perego1@aston.ac.uk (A.M. Perego).

https://doi.org/10.1016/j.optlaseng.2024.108040
Received 17 August 2023; Received in revised form 20 December 2023; Accepted 10 January 2024
Available online 2 February 2024

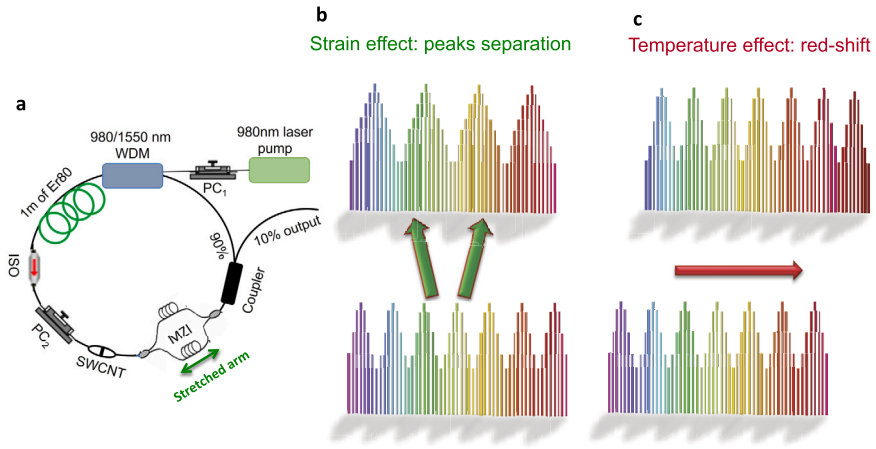

Fig. 1. Sensor concept and experimental setup. **a** Schematic of experimental setup: a ring fibre laser consisting of a passive fibre (black line), Erbium-doped fibre gain medium (Er80, green line) pumped by 980 nm laser (green rectangle) through a wavelength division multiplexer (WDM, grey rectangle), isolator (ISO), carbon nanotube saturable absorber (SWNCT), polarisation controllers (PC1,2) isolator (black rectangle) and Mach-Zehnder Interferometer (MZI). **b** The laser optical spectrum, resulting from intracavity pulse interference, exhibits spectral peaks grouping together multiple cavity modes: strain applied to the laser causes spectral peak separation; **c** temperature increase causes a collective spectral red-shift without affecting spectral peak separation.

and in optical time-domain reflectometry based strain sensing techniques [20], but never as the sensing element itself to the best of our knowledge.

2. Materials and methods

In this work we present a mode-locked all-fibre laser static strain sensor based on intracavity pulse interference. The sensor is environmentally stable, it does not require any external locking mechanism, and its strain response is decoupled from temperature variations due to a specific intracavity Mach-Zehnder interferometer (MZI) architecture. The key operational principle is as follows. A light pulse generated in a passively mode-locked laser is split into two pulses (OFCs) at the intracavity MZI input, and the two pulses travel inside the MZI along slightly different optical paths, interfering and recombining at the MZI output (the setup is shown in Fig. 1a). The resulting structure of the laser optical spectrum consists of multiple equally spaced peaks due to the mutual interference through the MZI, where each peak envelope contains several cavity modes. A similar multi-peak structure also manifests in the RF domain. Strain, applied by stretching one of the MZI arms, causes a change in the interference pattern, inducing a separation of the relative peaks in both the laser optical spectrum and RF spectrum, thus enabling sensing capability (see Fig. 1b). In contrast, temperature variations cause a collective red- or blue-shift of the whole optical spectrum without affecting the relative separation between peaks, as shown in Fig. 1c. In this way, temperature and strain effects are decoupled. As a comparison, traditional dual-comb measurement techniques employ two synchronised OFCs, generated by different sources, which interfere at a photo-detector following interaction between one of the OFCs and the sample to be measured or characterised e.g. in spectroscopy applications. A key novelty of our setup centres on the existence of a spectral interference pattern inside the cavity and it is the sensitivity of this interference pattern that enables sensing capabilities.

We have built a net anomalous dispersion ring cavity fibre laser using a 7.1 m long single mode optical fibre with nonlinearity $\gamma = 2\ \mathrm{km}^{-1}\ \mathrm{W}^{-1}$ and group velocity dispersion $\beta_2 = -20\ \mathrm{ps}^2\ \mathrm{km}^{-1}$ at 1550 nm wavelength. The gain medium comprises a 1 m long high concentration Erbium-doped fibre (Liekki Er80-8/125) pumped by a 980 nm laser diode. A polarisation controller (PC) is used to tune the polarisation cavity state, while a 51 dB dual-stage polarisation-independent optical isolator (ISO) is inserted in the laser cavity to ensure unidirectional propagation. A single-wall carbon nanotube (SWCNT) is used to achieve mode-locking operation. A 90:10 coupler allows extraction of 10% of the intracavity power, which is directed to a 2.5 GHz bandwidth oscilloscope (Tektronix DPO7254), to a 20 pm resolution (Yokogawa AQ6317B) optical spectrum analyser (OSA), and to a 13.6 GHz bandwidth RF analyser (Rohde & Schwarz) with 3 Hz resolution bandwidth, to characterise the laser output. We implemented an intracavity MZI with 2 m long arms using two 50:50 fibre couplers.

3. Results

We observed stable fundamental mode-locking when either arm of the interferometer was connected to the cavity in isolation. The recorded optical spectra – corresponding to each pulse – were centred at approximately 1559 nm, as shown in Fig. 2a; note that individual comb lines of each spectrum could not be visualised as their spacing is smaller than the OSA resolution. In this scenario, a single pulse circulating inside the laser was observed, having repetition rates of 20.4415 MHz and 20.4465 MHz (see Fig. 2b), depending on which arm was connected, and corresponding to total cavity lengths of 10.14238 m and 10.1399 m respectively. The oscilloscope temporal traces showing the two light pulses are plotted in Fig. 2c.

When both MZI arms were connected to the cavity with a path difference of about 2.48 mm, we could observe the signatures of the two pulses/OFCs interference in both the optical and RF spectrum with a separation between consecutive peaks of 0.715 nm (Fig. 2d) and 45.7 kHz (Fig. 2e) respectively. The optical spectrum peaks are determined by the maxima of the MZI transmission function (assuming the linear phase-shift as the leading contribution, this yields a spacing $\Delta\lambda = \lambda^2/(n_g \Delta\mathcal{L}) \approx 0.7$ nm with $\lambda = 1560$ nm, MZI arm length difference $\Delta\mathcal{L} = 2.48$ mm, and group index $n_g = 1.4$). We highlight the excellent noise properties of the interference spectrum which enable clear identification of the individual spectral features: the FWHM bandwidth of the optical and RF beat note is approximately 56 pm and 8 kHz respectively, with a high signal-to-noise-ratio (SNR) of about 60 dB and 50 dB respectively. Fig. 2f and its inset show the temporal trace extracted at the cavity output coupler, consisting in an amplitude envelope which modulates – on a time scale of the order of 20 μs corresponding to the inverse of the RF spectrum linespacing – a train of pulses repeating with the cavity round trip time periodicity of about 50 ns. To test the mode-locked laser strain sensing capabilities, we extended one arm of the MZI (the 'sensor arm') by ΔL using a micrometre bonded to the fibre with a gauge length of $L = 0.1$ m. The resulting strain can be defined as $\Delta L/L$. The applied strain induces a change in the delay of the sensor arm pulse only, which in turn translates into a change of the

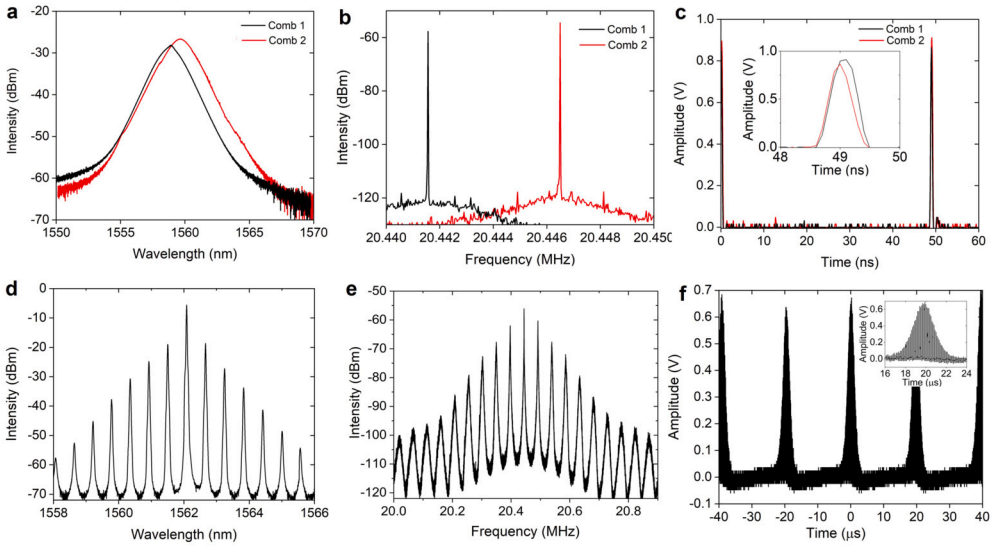

Fig. 2. Laser operational regimes characterisation. **a** Optical spectrum, **b** RF beat note, **c** oscilloscope temporal trace corresponding to fundamental mode-locking when either arm of the MZI is connected to the laser cavity in isolation. **d** Optical spectrum, **e** RF spectrum, and **f** oscilloscope temporal trace showing interference when both MZI arms are connected to the laser cavity.

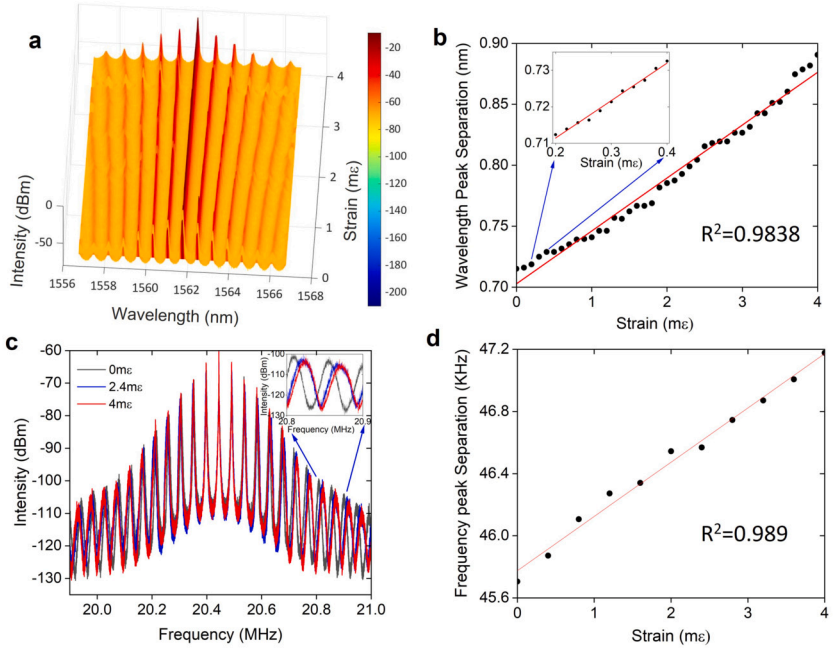

Fig. 3. Strain sensing performances. **a** 3D contour plot showing how peak separation in the optical spectrum increases proportionally to applied strain. **b** Linear fit showing the relationship between applied strain and spectral peak separation (43 pm/mϵ sensitivity obtained from fit slope), the inset depicts a finer resolution zoom. **c** RF spectrum recorded for 3 different values of applied strain (see legend), the inset depicts a zoom highlighting changes due to different strain applied. **d** Linear fit of RF spectral separation versus applied strain (350 Hz/mϵ sensitivity from fit slope).

relative peak separation in both the optical and RF spectra, as shown in Figs. 3a and 3c respectively. For each value of strain applied, the spectral spacing is calculated as the average spacing between closest neighbour peaks in the optical and RF spectrum respectively, considering only the peaks with height exceeding the noise floor by more than 10 dBs: this corresponded to approximately 30/20 peaks per recorded spectrum respectively. As the strain applied to the laser causes separation of spectral peaks, the spectral resolution of the optical spectrum analyser or RF analyser used ultimately limits the fine tracking of spectral peak position and hence strain measurement precision. In our work, averaging over multiple spectral peak separations reduces further possible errors in single peak tracking. The optical wavelength and RF peaks separation increased linearly with a change in strain, with a sensitivity of 43 pm/mϵ and 350 Hz/mϵ respectively over a strain range of 4 mϵ (see Figs. 3b and 3d). In Fig. 3b and 3d we show that the spectral response is linear with respect to the applied strain over a 4 mϵ range, both for optical and RF spectrum. The inset of Fig. 3b shows a finer scan demonstrating 20 $\mu\epsilon$ resolution. The achieved resolution was limited by the smallest increment of the micrometre to apply strain rather than the proposed sensing method. Further improvements in sensor performance could be achieved by applying the strain with more advanced methods such as using high precision motorised stage systems with longer gauge lengths, and it will be the subject of future work. We have studied the impact of temperature variations on the strain sensing capabilities of our device by increasing temperature in the MZI sensor arm, starting from lab background level (~27 °C) to approximately 53 °C using a

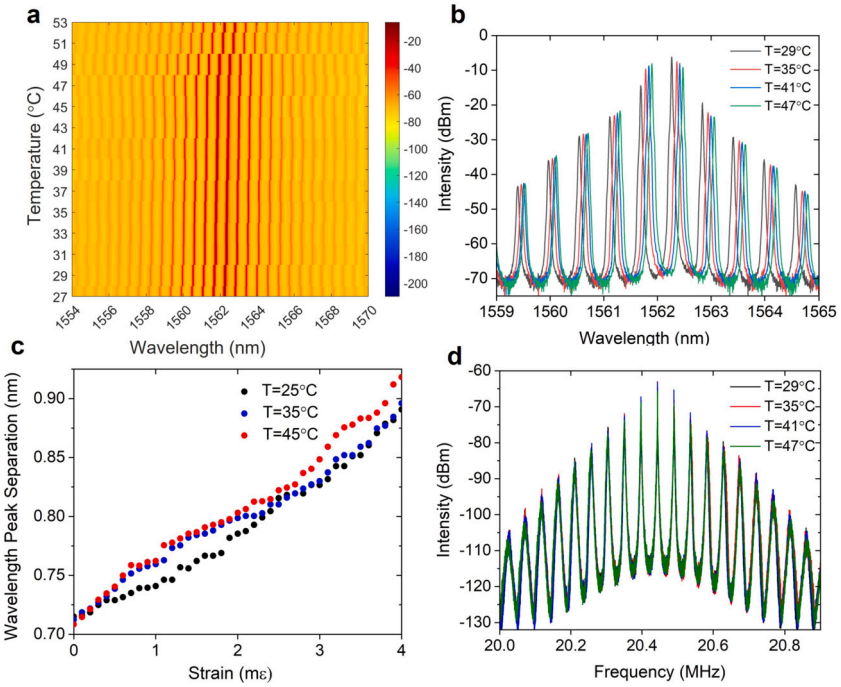

Fig. 4. Temperature effect on the measured optical spectrum. a The optical spectrum shifts rigidly as a function of increasing temperature. **b** Examples of optical spectra taken at different temperature levels (see legend). **c** Optical spectral peak separation as a function of applied strain for 3 different temperature levels. **d** RF spectrum obtained for the same temperatures as in **b** (see legend).

Peltier element. From Figs. 4a and 4b, there is a rigid collective shift of the optical spectrum with an increase in temperature. From Fig. 4c it can be seen that different temperature levels have an insignificant influence on the linearity and sensitivity of the relationship between applied strain and peak separation. Temperature has no relevant influence on the RF spectral peak separation either as it can be appreciated from Fig. 4d. Furthermore, a global temperature change affecting both MZI arms simultaneously, which is the most likely scenario to occur in applications as the whole device would be immersed in a common environment, will not have an impact on the spectral peaks separation as the interference properties depend on relative changes of optical path between the two MZI arms. Spectral fringes drift due to temperature in MZI devices has been extensively investigated in the literature [38–42]. In silica fibres this drift is caused by thermal dependence of the refractive index, and an analytical estimate of the phase shift can be obtained by differentiating the accumulated phase (or group delay) with respect to temperature and considering measured values of the thermo-optic and thermal expansion coefficients [39,40]. Mitigation strategies for this effect have been proposed too. However, in our setup the global drift is not disturbing the operation of the sensor as strain is causing changes in the relative position of the spectral peaks and not a drift. Furthermore, possible residual changes in the relative position of the peaks caused by temperature, if present, are negligible in magnitude compared to that caused by strain.

We have investigated the spectral stability of the laser for a fixed level of applied strain. The corresponding temporal evolution of optical and RF spectra is depicted in Fig. 5a and 5b respectively. Data were obtained performing one acquisition of RF and OSA spectrum respectively every 5 minutes for 60 minutes, corresponding to a total of 12 measurements. The results show that the optical and RF beat notes are stable and experience negligible changes over the time interval considered. We have measured the temporal evolution of the average peak spectral separation, which is the physical observable associated to strain sensing, and obtained a standard deviation of 0.95 pm for optical spectrum and 5.55 Hz for RF spectrum (see Supplementary Material for more details). While one can not a priori exclude spectral changes between consecutive measurements, taking stability measurements with this granularity was motivated by the fact that during the laser operation we never observed any abrupt change in its emission spectral properties. The experiment was also executed multiple times to quantify the repeatability of the sensor performance: the standard deviations for the RF and optical measurements are ∼0.1 kHz and ∼0.01 nm respectively, as shown Fig. 5c and 5d, and have been obtained from 5 data points for each value of applied strain.

4. Discussion

The proposed sensor presents significant advantages over alternative photonic-based strain sensing technologies in that it overcomes the limitation of coupled temperature-strain sensitivity; despite the fact that improvements are still needed to achieve resolution of the order of few $n\epsilon$ like for instance in [34]. Ideally, and particularly for civil engineering applications, the sensor resolution would require improvement to achieve the micro-strain or even few hundreds of nano-strain level. To improve the resolution limit one could either increase the gauge length L, hence making the MZI arms longer, or reducing ΔL. While increasing L too much (e.g. by several meters) will substantially affect the overall laser performance, the most suitable way would consist in using a more fine grained approach to stretch the fibre (e.g. by means of a motorised high precision micrometer) providing changes in strain in much smaller steps. Compared to other approaches where dual-comb sources have been employed to interrogate FBGs [32–36], our solution decouples temperature and strain effects. This is because having FBGs as sensing elements does not eliminate temperature-strain crosstalk, irrespective from the fact that the dual-comb source used to interrogate them may be thermally stable or not. Furthermore, our sensor is environmentally stable and does not require complicated alignment and synchronisation procedures [30,31,43]. As it can be built with low-cost commercially available components, it does not require ad hoc fabrication techniques either [44]. Compared to alternative non-mode-locked MZI based laser sensors [45], our solution avoids the need for a second interferometer or speciality multicore fibre hence providing reduced complexity. An additional advantage of the proposed sensor compared to other optical platforms relying on single wavelengths in-

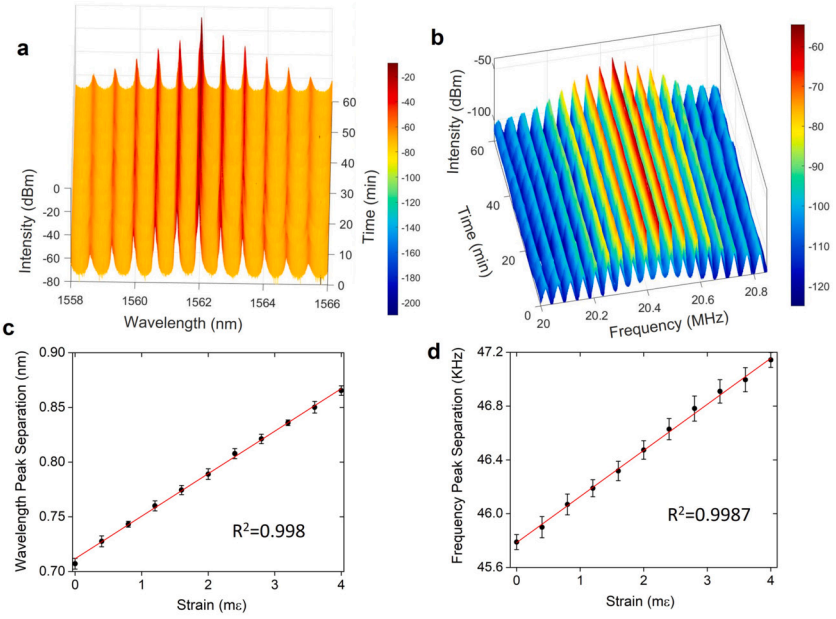

Fig. 5. Sensor stability and repeatability. **a** Optical spectrum, and **b** RF spectrum stability measured over time at constant strain. Repeatability of sensor performances quantified from standard deviation over multiple measurements for **c** optical spectrum and **d** RF spectrum respectively.

terrogation such as FBGs or non-mode-locked lasers, relates to the RF domain readout and the potential reduction in readout errors too, as the sensor output uses a statistical average over multiple spectral features. We stress the fact that, while we have presented here results about the sensor interrogation both from RF and optical spectrum to provide a more complete characterisation of the device, from applications point of view the RF domain interrogation is preferable due to lower costs (for instance using commercially available portable RF spectrum analysers).

The sensor performance should be immune from undesired effects due to group velocity mismatch for realistic operational configurations. Indeed group velocity mismatch resulting from different lengths of the two MZI arms – in case of very large optical path length – may affect the possibility of interference between optical pulses travelling along the two different arms. Our results suggest that with the present setup, strain sensing in the millistrain and in the few tens of microstrain range can be easily and reliably achieved. Most devices used for monitoring strain in civil engineering applications are aiming at measuring strain changes with much higher resolution – of the order of the microstrain or below – which means that the path length difference will be much smaller than what we considered in this work. Hence we would expect that group velocity mismatch between the two arms will not have a relevant impact on the sensor performance.

Our innovation creates new possibilities for robust temperature-insensitive strain sensing for a wide range of practical applications currently under-served by existing temperature-prone commercial sensors. These areas include high value markets such as structural health monitoring of civil infrastructure, oil and gas drilling, nuclear, and industrial machining. The proposed approach can be also deployed to interrogate other physical parameters with insensitivity to temperature, including pressure, curvature, torsion and displacement.

5. Conclusions

In conclusion, we have presented a mode-locked fibre laser static strain sensor based on intracavity pulse interference, achieving 20 $\mu\epsilon$ resolution over a 4 mϵ range, with the minimum observed resolution limited by the strain steps achievable in the laboratory. Our stable, all-fibre architecture, decouples strain and temperature response, enables RF domain readouts and avoids the need for external stabilisation. These unique selling points pave the way for a new generation of low-cost and environmentally robust sensors suitable for deployment at scale in civil, mechanical and aerospace engineering. These markets are multi-billion dollar industries such that there is significant potential for future impact.

CRediT authorship contribution statement

Hani J. Kbashi: Conceptualization, Investigation, Methodology, Validation, Writing – review & editing. **Brian B. Sheil:** Conceptualization, Methodology, Writing – review & editing. **Auro M. Perego:** Conceptualization, Methodology, Supervision, Writing – original draft.

Declaration of competing interest

The authors declare that they have no known competing financial interests or personal relationships that could have appeared to influence the work reported in this paper.

Data availability

Data will be made available on request.

Acknowledgements

H.K. and A.M.P. acknowledge support from the EPSRC project EP/W002868/1. A.M.P. and B.S. acknowledge support from the Royal Academy of Engineering through the Research Fellowship scheme.

Appendix A. Supplementary material

In the Supplementary Material more information can be found on the laser stability.

Supplementary material related to this article can be found online at https://doi.org/10.1016/j.optlaseng.2024.108040.

References

[1] Lawson NJ, et al. Development and application of optical fibre strain and pressure sensors for in-flight measurements. Meas Sci Technol 2016;27:104001.
[2] Brownjohn J. Structural health monitoring of civil infrastructure. Philos Trans R Soc A, Math Phys Eng Sci 2007;365:589.

[3] Xiang J-W, Yang Z-B, Aguilar JL. Structural health monitoring for mechanical structures using multi-sensor data. Int J Distrib Sens Netw 2018;14:1550147718802019.
[4] Liu C, Teng J, Wu N. A wireless strain sensor network for structural health monitoring. Shock Vib 2015:740471.
[5] Deivasigamani A, Daliri A, Wang C, John S. A review of passive wireless sensors for structural health monitoring. Mod Appl Sci 2013;7:57.
[6] Royston R, Sheil BB, Byrne BW. Monitoring the construction of a large-diameter caisson in sand. Proc Inst Civ Eng Geotech Eng 2022;175:323.
[7] Majumder M, Gangopadhyay TK, Chakraborty AK, Dasgupta K, Bhattacharya D. Fibre Bragg gratings in structural health monitoring - present status and applications. Sens Actuators A, Phys 2008;147:150.
[8] Soga K, Luo L. Distributed fiber optics sensors for civil engineering infrastructure sensing. J Struct Integr Maint 2018;3:1.
[9] Glisic B, Inaudi D. Fibre optic methods for structural health monitoring. John Wiley & Sons; 2008.
[10] Grattan K, Sun T. Fiber optic sensor technology: an overview. Sens Actuators A, Phys 2000;82:40.
[11] Fortier T, Baumann E. 20 years of developments in optical frequency comb technology and applications. Commun Phys 2019;2:153.
[12] Rieker GB, et al. Frequency-comb-based remote sensing of greenhouse gases over kilometer air paths. Optica 2014;1:290.
[13] Coddington I, Swann W, Nenadovic L, Newbury NR. Rapid and precise absolute distance measurements at long range. Nat Photonics 2009;3:351–6.
[14] Udem T, Holzwarth R, Hänsch TW. Rapid and precise absolute distance measurements at long range. Nature 2002;416:233–7.
[15] Piqué N, Holzwarth R, Hänsch TW. Frequency comb spectroscopy. Nat Photonics 2019;13:146–57.
[16] Spencer DT, et al. An optical-frequency synthesizer using integrated photonics. Nat Photonics 2018;557:81–5.
[17] McCracken RA, Charsley JM, Reid DT. A decade of astrocombs: recent advances in frequency combs for astronomy. Opt Express 2017;25:15058.
[18] Suh MG, et al. Searching for exoplanets using a microresonator astrocomb. Nat Photonics 2019;13:25–30.
[19] Hu H, et al. Single-source chip-based frequency comb enabling extreme parallel data transmission. Nat Photonics 2018;12:469–73.
[20] Soriano-Amat M, et al. Time-expanded phase-sensitive optical time-domain reflectometry. Light: Sci Appl 2021;10:51.
[21] Gaeta AL, Lipson M, Kippenberg TJ. Photonic-chip-based frequency combs. Nat Photonics 2019;13:158.
[22] Pasquazi A, et al. Micro-combs: a novel generation of optical sources. Phys Rep 2018;729:1. micro-combs: a novel generation of optical sources.
[23] Yang T, Dong J, Liao S, Huang D, Zhang X. Comparison analysis of optical frequency comb generation with nonlinear effects in highly nonlinear fibers. Opt Express 2013;21:8508.
[24] Parriaux A, Hammani K, Millot G. Electro-optic frequency combs. Adv Opt Photonics 2020;12:223.
[25] Kobayashi Y, et al. Femtosecond optical parametric oscillator frequency combs. J Opt 2015;17:094010.
[26] Bao H, et al. Laser cavity-soliton microcombs. Nat Photonics 2019;13:384–9.
[27] Rowley M, et al. Self-emergence of robust solitons in a microcavity. Nature 2022;608:303–9.
[28] Cundiff ST, Ye J. Colloquium: femtosecond optical frequency combs. Rev Mod Phys 2003;75:325.
[29] Coddington I, Newbury N, Swann W. Dual-comb spectroscopy. Optica 2016;3:414.
[30] Minamikawa T, et al. Strain sensing based on strain to radio-frequency conversion of optical frequency comb. Opt Express 2018;26:9484.
[31] Lu X, et al. Ultrasensitive, high-dynamic-range and broadband strain sensing by time-of-flight detection with femtosecond-laser frequency combs. Sci Rep 2017;7:13305.
[32] Guo J, Ding Y, Xiao X, Kong L, Yang C. Multiplexed static fbg strain sensors by dual-comb spectroscopy with a free running fiber laser. Opt Express 2018;26:16147.
[33] Zhao K, et al. Free-running dual-comb fiber laser mode-locked by nonlinear multimode interference. Opt Lett 2019;44:4323.
[34] Kuse N, Ozawa A, Kobayashi Y. Static fbg strain sensor with high resolution and large dynamic range by dual-comb spectroscopy. Opt Express 2013;21:11141.
[35] Zhang R, Zhu Z, Wu G. Static pure strain sensing using dual-comb spectroscopy with fbg sensors. Opt Express 2019;27:34269.
[36] Posada-Roman JE, Garcia-Souto JA, Poiana DA, Acedo P. Fast interrogation of fiber Bragg gratings with electro-optical dual optical frequency combs. Sensors 2016;16. https://doi.org/10.3390/s16122007.
[37] Zhao X, et al. Dynamic quasi-distributed ultraweak fiber Bragg grating array sensing enabled by depth-resolved dual-comb spectroscopy. IEEE Trans Instrum Meas 2020;69:5821.
[38] Lagakos N, Bucaro JA, Jarzynski J. Temperature-induced optical phase shifts in fibers. Appl Opt 1981;20:2305.
[39] Slavík R, et al. Ultralow thermal sensitivity of phase and propagation delay in hollow core optical fibres. Sci Rep 2015;5:15447.
[40] Shi B, et al. Temperature insensitive delay-line fiber interferometer operating at room temperature. J Lightwave Technol 2022;40:5716.
[41] Zhu W, Fokoua ERN, Chen Y, Bradley T, Petrovich MN, Poletti F, et al. Temperature insensitive fiber interferometry. Opt Lett 2019;44:2768.
[42] Tang L, Li Y, Li J, Yang S, Chen H, Chen M. Temperature-insensitive Mach–Zehnder interferometer based on a silicon nitride waveguide platform. Opt Lett 2020;45:2780.
[43] Dong Y, Chen X, Liu E, Fu C, Zhang H, Lu Z. Quantitative measurement of dynamic nanostrain based on a phase-sensitive optical time domain reflectometer. Appl Opt 2016;55:7810.
[44] Gong Y, et al. Temperature-insensitive micro Fabry–Pérot strain sensor fabricated by chemically etching er-doped fiber. IEEE Photonics Technol Lett 2009;21:1725.
[45] Zhang L, et al. Room-temperature power-stabilized narrow-linewidth tunable erbium-doped fiber ring laser based on cascaded Mach-Zehnder interferometers with different free spectral range for strain sensing. J Lightwave Technol 2020;38:1966.